Inorganic Chemistry

pubs.acs.org/IC

Article

Mono- and Disamarium Azacryptand Complexes: A Platform for Cooperative Rare-Earth Metal Chemistry

Johanna M. Uher, Matthias R. Steiner, and Johann A. Hlina*

Cite This: *Inorg. Chem.* 2022, 61, 5539−5546

Read Online

ACCESS | Metrics & More | Article Recommendations | Supporting Information

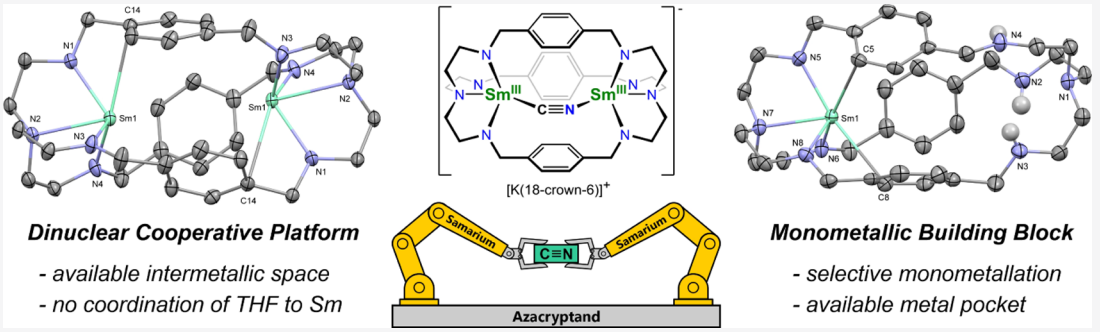

ABSTRACT: Mono- (H_3LSm) and disamarium complexes (LSm_2) were prepared by reaction of the azacryptand $N[(CH_2)_2NHCH_2\text{-}p\text{-}C_6H_4CH_2NH(CH_2)_2]_3N$ (H_6L) with 1 or 2 equiv of $Sm[N(SiMe_3)_2]_3$, respectively. The disamarium complex features free coordination sites on both metal centers available for bridging ligands shielded by phenylenes from tetrahydrofuran (THF) coordination. The reaction of LSm_2 with KCN and 18-crown-6 yielded the adduct $[LSm_2\text{-}\mu\text{-}\eta^1\text{:}\eta^1\text{-}CN][K(18\text{-crown-}6)(THF)_2]$ featuring a bridging cyanide. The complexes were characterized by crystallography, electrochemical analysis, NMR, and optical spectroscopy, and the effective magnetic moments were determined via the Evans method.

INTRODUCTION

The organometallic chemistry of f-block metals exhibits numerous examples in which two monometallic complexes engage in cooperative activation of substrate molecules. Prominent examples in the context of small inert molecules involve reductive coupling of carbon monoxide,[1−6] dinitrogen reduction,[7−9] and sulfur dioxide coordination.[10] Among the rare-earth metals, samarium is a key player in small molecule activation. Typically, two monometallic complexes react with the substrate and form a dinuclear complex in which the two metal ions are bridged by the converted substrate. Using such reactions as a basis for the development of catalytic processes, it appears feasible to utilize ligand frameworks, which already provide a link between the two metal centers. In f-metal chemistry, the number of complexes featuring such an architecture is limited and macrocyclic ligands are most prominent. Here, the so-called Pacman ligands have proven valuable in studying the cooperative chemistry of f-metal ions. The groups of Arnold and Love have reported examples exploring the cooperative interaction of f-block metals with uranium at the center of attention.[11−14] Macrocyclic azacryptands have been introduced by Lehn and co-workers and the derivatives in which the two tris(2-aminoethyl)amine (TREN) moieties are bridged with phenylenes are ideal ligand frameworks to study cooperative reactivity of dinuclear complexes.[15] Previously, investigations of such azacryptands focussed on late transition metals and include examples of cooperative interaction such as catalytic carbon dioxide conversion using a dinickel complex.[16] TREN-based ligands have successfully demonstrated their utility in f-metal chemistry already as exemplified by complexes featuring unusual moieties such as the terminal nitride[17] or oxide[18] as well as engaging in reductive carbon monoxide coupling[19] and metal−metal bonding.[20] Here, we present samarium compounds as the first examples of mono- and dinuclear f-metal azacryptand complexes.

RESULTS AND DISCUSSION

Synthesis and Characterization. The disamarium azacryptand complex LSm_2, **1**, was prepared by heating the azacryptand ligand H_6L (H_6L = $N[(CH_2)_2NHCH_2\text{-}p\text{-}C_6H_4CH_2NH(CH_2)_2]_3N$) with 2 equiv of $Sm[N(SiMe_3)_2]_3$ to 80 °C in tetrahydrofuran (THF) (Scheme 1). During the reaction, **1** precipitated in the form of a yellow powder, which

Received: December 24, 2021
Published: March 28, 2022

https://doi.org/10.1021/acs.inorgchem.1c03989
Inorg. Chem. 2022, 61, 5539−5546

Scheme 1. Preparation of the Azacryptand Disamarium (1) and Monosamarium (2) Complexes as well as the Synthesis of the Azacryptand Disamarium Complex Cyanide Adduct $[LSm_2\text{-}\mu\text{-}\eta^1{:}\eta^1\text{-}CN][K(18\text{-Crown-6})(THF)_2]$ (3)

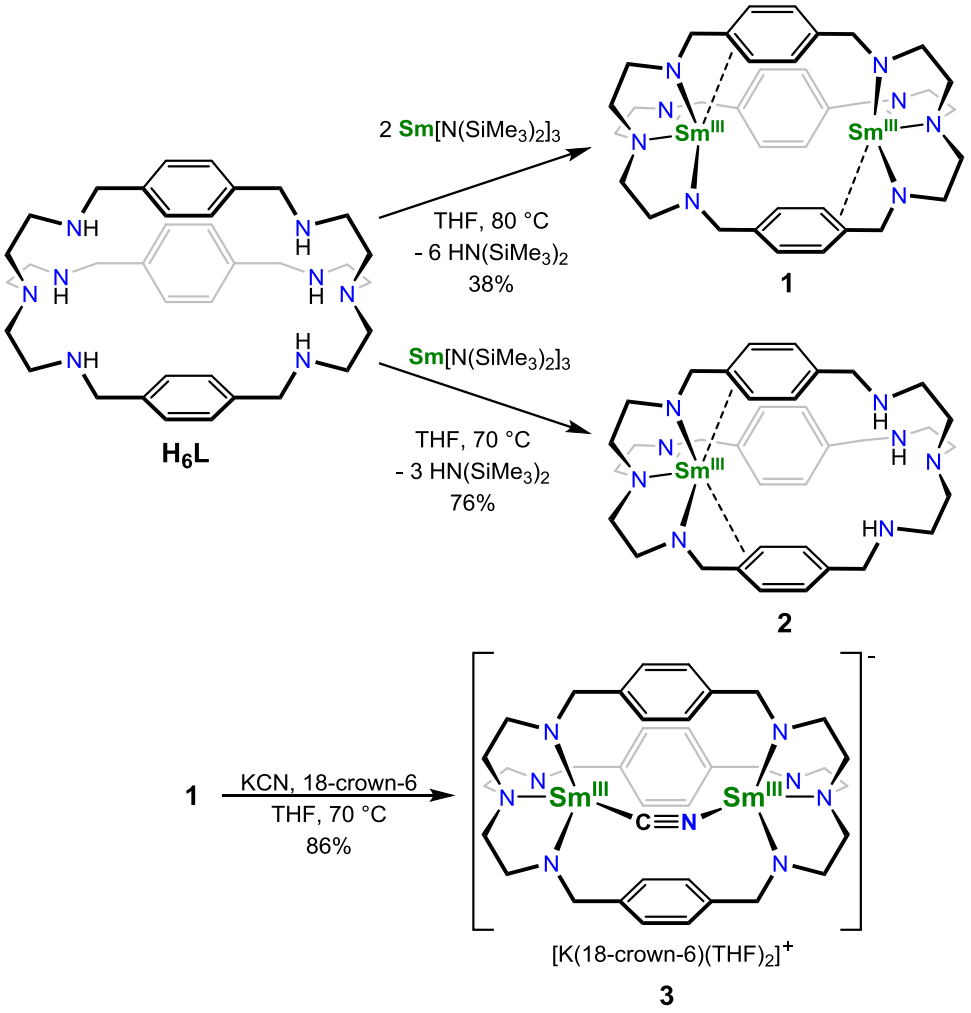

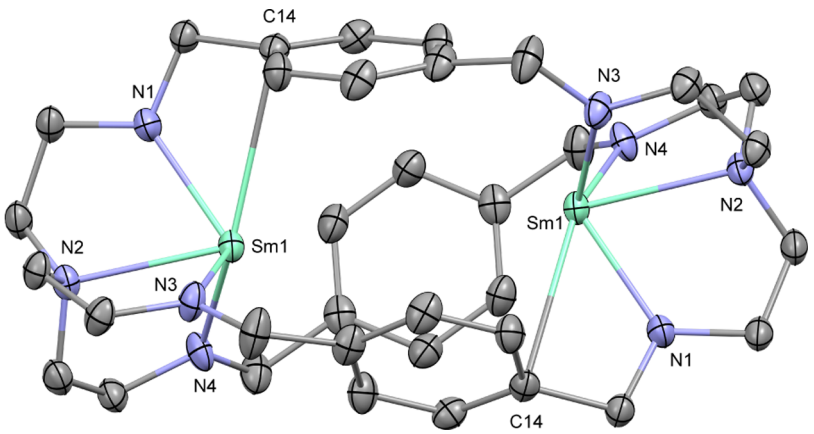

Figure 1. Molecular structure of **1**. Hydrogen atoms are omitted for clarity. Thermal ellipsoids drawn at 50% probability. Selected distances (Å) and angles (deg): Sm1−N1: 2.247(4), Sm1−N2: 2.514(4), Sm1−N3: 2.260(5), Sm1−N4: 2.244(5), Sm1−C14: 3.056(5), Sm1···Sm1′: 5.1758(9), N1−Sm1−N2: 68.6(1), N2−Sm1−N3: 69.7(1), and N2−Sm1−N4: 70.2(1).

was subsequently isolated in 38% yield. The solubility of **1** is low in DME, toluene, and benzene, and **1** is insoluble in pentane and diethyl ether. Along with the dinuclear samarium complex **1**, we also observed the mononuclear intermediate H_3LSm, **2**, as a side-product of the reaction, which precipitated along with **1**. Multiple washings of the crude product with THF were done to remove **2**. The washing also accounts for the loss of **1** and its low isolated yield.

Single-crystal X-ray diffraction analysis of a yellow crystal of **1** confirmed the bimetallic structure of the complex (Figure 1). Each of the two samarium(III) ions occupies one of the TREN pockets and they exhibit an intermetallic distance of 5.1758(9)

https://doi.org/10.1021/acs.inorgchem.1c03989
Inorg. Chem. 2022, 61, 5539−5546

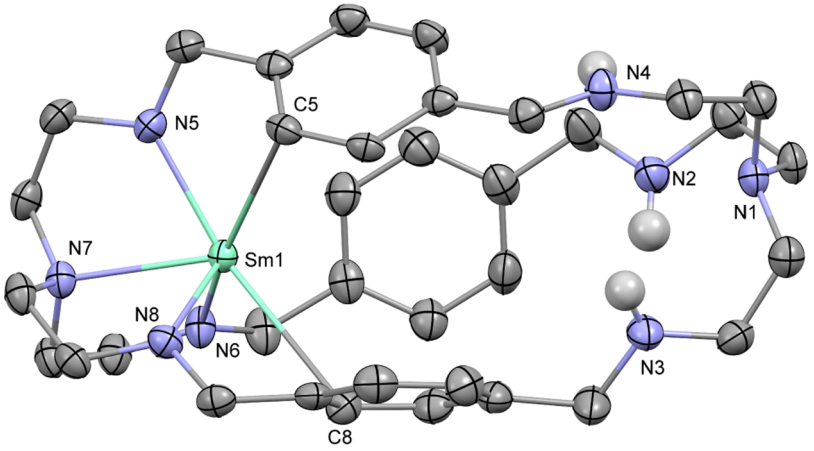

Figure 2. Molecular structure of **2**. Selected hydrogen atoms are omitted for clarity. Thermal ellipsoids drawn at 50% probability. Selected distances (Å) and angles (deg): Sm1−N5: 2.270(4), Sm1−N6: 2.280(3), Sm1−N8: 2.276(3), Sm1−N7: 2.521(4), Sm1−C5: 3.060(4), Sm1−C8: 3.070(5), N5−Sm1−N7: 69.4(1), N6−Sm1−N7: 69.7(1), and N7−Sm1−N8: 69.6(1).

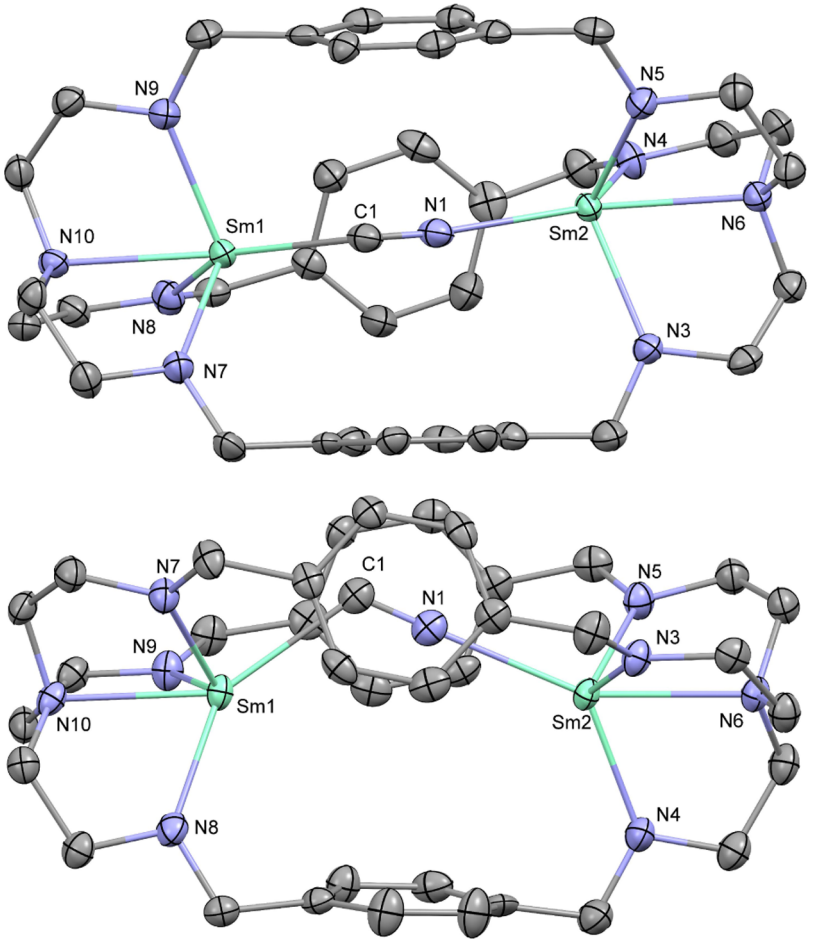

Figure 3. Molecular structure of an anionic substructure of **3** in side and top views. Hydrogen atoms and additional disordered cyanide are omitted for clarity. Thermal ellipsoids drawn at 50% probability. Selected distances (Å) and angles (deg): C1−N1: 1.20(2), Sm1−C1: 2.52(2), Sm2−N1: 2.56(1), Sm1−N7: 2.279(5), Sm1−N8: 2.312(6), Sm1−N9: 2.320(6), Sm1−N10: 2.526(4), Sm2−N3: 2.312(6), Sm2−N4: 2.306(5), Sm2−N5: 2.290(6), Sm2−N6: 2.533(4), Sm1···Sm2: 5.512(1), Sm1−C1−N1: 121(1), and Sm2−N1−C1: 175(1).

Å. The ligand framework is "twisted" along the metal−metal axis, which indicates a certain degree of flexibility. The distances of samarium to the amide nitrogen atoms are in the range of 2.244(5)−2.260(5) Å and those to the tertiary nitrogen atom are 2.514(4) Å. Each samarium center exhibits π-interaction with one of the bridging phenylenes with a short Sm1−C14 distance of 3.056(5) Å, which is well within the sum of the van der Waals radii of samarium and carbon of 4.67 Å.[21] The solid-state structure also revealed vacant space in between the two samarium centers with available coordination sites along the metal−metal axes without any THF coordinated to the samarium ions, despite its use as a solvent in the

https://doi.org/10.1021/acs.inorgchem.1c03989
Inorg. Chem. 2022, 61, 5539−5546

preparation. This renders this compound an ideal platform to study the cooperative interaction with small molecules. As we observed the formation of the monometallated intermediate **2** in the synthesis of **1**, we were prompted to investigate the selective synthesis of the monosamarium derivative. Changing the stoichiometry to using equimolar amounts of H_6L and $Sm[N(SiMe_3)_2]_3$ under similar conditions yielded the monosamarium complex **2** selectively. Crystallization from hot benzene gave **2** as orange crystals in 76% isolated yield.

This method also yielded crystals suitable for X-ray diffraction analysis and the molecular structure confirmed that only one of the TREN moieties was coordinated with a samarium ion (Figure 2). The distances of the samarium ion to the amide nitrogen atoms are in the range from 2.270(4) to 2.280(3) Å and the distance to the tertiary nitrogen atom is 2.521(4) Å, which is in both cases slightly longer than what was observed in **1**. With the second TREN pocket not being occupied, the one samarium center exhibits an interaction with two of the phenylenes with short Sm−C distances at 3.060(4) (C5) and 3.070(5) Å (C8). Interestingly, only two other monometallic complexes featuring this azacryptand ligand have been reported so far with cobalt.[22] To assess the possibility of intermolecular metal ion exchange, we heated a solution of **2** in benzene to 70 °C for 1 day, but did not observe significant redistribution to **1** and H_6L.

With the intermetallic space in the dinuclear complex **1** being available for coordination, we probed the cooperative ligand binding with cyanide, which is isoelectronic to carbon monoxide and dinitrogen. For this purpose, we treated **1** with equimolar amounts of potassium cyanide and 18-crown-6 at 70 °C. Heating was required due to the low solubility of potassium cyanide in THF even in the presence of crown ether and was applied until all of it was consumed, which was typically within 2 h. This yielded the cyanide adduct $[LSm_2\text{-}\mu\text{-}\eta^1{:}\eta^1\text{-}CN][K(18\text{-crown-}6)(THF)_2]$ (**3**) as yellow crystals in 86% after crystallization from THF/diethyl ether at −50 °C. The ion-separated compound is insoluble in aromatic and aliphatic solvents but readily dissolves in THF in contrast to its parent compound **1**.

Crystals of the cyanide adduct **3** suitable for single-crystal X-ray diffraction were grown from a highly concentrated solution in THF at ambient temperature. The solid-state structure of **3** (Figure 3) shows the compound as a coordination polymer with the $[LSm_2\text{-}\mu\text{-}\eta^1{:}\eta^1\text{-}CN]^-$ fragments being bridged with $[K(18\text{-crown-}6)]^+$ groups and the asymmetric unit contains two sets of each fragment (see Figure S1). Within the rare-earth metal fragments, the bridging cyanide groups are not directly on the metal−metal axis but slightly "pushed out" of the center of the complexes and in between two of the bridging phenylenes, which are oriented almost co-planar. The ligand frameworks are stretched out with Sm···Sm distances extended from 5.1758(9) Å in **1** to 5.463(1)−5.512(1) Å in **3**. The cyanides are coordinated to both the rare-earth metal centers and are disordered. Previously reported multinuclear samarium(III) complexes featuring bridging cyanides exhibited nearly linear Sm−CN−Sm axes.[23−27] Since the intermetallic distance is controlled by the ligand framework and is too short to support a linear arrangement, the cyanide appears in a range of orientations to adopt nearly linear coordination with either of the two metal centers. Modeling the disordered cyanides resulted in nearly linear arrangement of the cyanides with one of the two samarium atoms as depicted in Figure 3 with one of the two disordered cyanide groups. Refinement of these linear arrangements as N−C−Sm or C−N−Sm did not exhibit significant differences in the *R*-factor values, rendering them indistinguishable. DFT calculations by Yang and co-workers on fullerene-encapsulated yttrium and terbium cyanide compounds, in which the carbon and nitrogen atoms of the cyanides were also indistinguishable by X-ray diffraction analysis, showed the C−N−Ln arrangement in nearly linear coordination to be more stable than the N−C−Ln arrangement.[28] Thus, we assigned carbon and nitrogen for near linear coordination to one samarium via the nitrogen atom (C1−N1−Sm2 in Figure 3) and the bent coordination (Sm1−C1−N1 in Figure 3) to the other samarium atom via the carbon atom. The bond distances between the cyanide nitrogen and the samarium atoms are in the range of 2.49(3)−2.56(1) Å, of which the N1−Sm2 bond depicted in Figure 3 represents the upper end, and the $Sm-C_{CN}$ distances range from 2.47(7) to 2.52(2) Å, of which the Sm1−C1 bond depicted in Figure 3 exhibits the longest distance (see Figure S1 for the remaining $Sm-N_{CN}$ and $Sm-C_{CN}$ bond distances). These bond distances are similar to previously reported examples for crystallographically characterized compounds featuring cyanides bridging two samarium ions.[23−27] The C−N bond distances in the cyanides are in the range of 1.17(7)−1.20(2) Å and a corresponding IR stretch vibration is observed at 2116 cm^{-1} (see Figure S18). In comparison to **1**, the distances of the samarium atoms to the amide nitrogen atoms are elongated and in the range of 2.281−2.325 Å and those to the tertiary nitrogen atoms in the range of 2.510(6)−2.533(4) Å.

Spectroscopy. The ^1H NMR spectroscopic analysis of **1** showed three broadened and paramagnetically shifted resonances at −10.23, −3.06, and 6.53 ppm, of which we assigned the two former to the methylene groups in the TREN moieties and the latter to the phenylene-bound methylene groups. The resonance of the bridging phenylenes is not observed. Even after prolonged measurement time, no ^{13}C NMR data could be recorded for **1**. Using the Evans method, we calculated the effective magnetic moment, μ_{eff}, of **1** to be 2.35 μ_B.[29] This is comparably low for a dinuclear compound considering that a typical range for samarium(III) compounds was reported at 1.4−1.7 μ_B.[30] The absence of the second paramagnetic samarium(III) center in **2** is reflected in a symmetry break and a declining paramagnetic influence toward the unoccupied ligand pocket. The strongly paramagnetically shifted resonances range from −8.00 to 11.37 ppm. Among the nine resonances, the ones at −8.00, −1.29, and 1.65 ppm, which we assigned to the methylene of the samarium-coordinated TREN moiety, are strongly broadened and partially exhibit too low integrals in comparison with the other signals. The effective magnetic moment of the mononuclear complex was calculated to be μ_{eff} = 1.80 μ_B. This is considerably higher than expected, when comparing this with the dinuclear derivative **1** and might indicate magnetic interaction of the two metal centers in **1**. In case of **3**, the introduction of the cyanide group into **1** results in a more rigid structure, which is also reflected in the NMR data with less strongly broadened signals. The ^1H NMR resonances observed for **3** are significantly less paramagnetically shifted when compared with the parent complex **1** with the four signals of the *ate*-complex covering a range from −4.91 to 5.97 ppm. Along with the broadened methylene resonances at −4.91, −0.14, and 5.13 ppm, the narrow resonance for the phenylene protons is now observed at 5.97 ppm. Considering that the solid-state structure would suggest symmetry breaks

https://doi.org/10.1021/acs.inorgchem.1c03989
Inorg. Chem. 2022, 61, 5539−5546

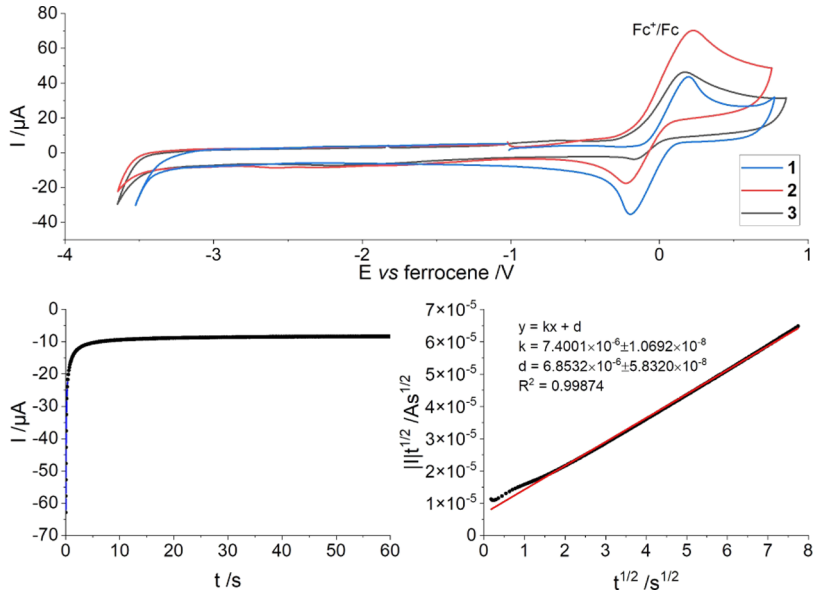

Figure 4. Top: Cyclic voltammetry of compounds **1**, **2**, and **3**. Data recorded from 2 mM solutions of both analyte and ferrocene in THF using $^{n}Bu_4NPF_6$ (100 mM) at scan rates of 50 (**2** and **3**) or 100 mVs^{-1} (**1**). Bottom left: Chronoamperometric data for **1** using a potential of −3.3 V vs Fc^+/Fc for 60 s and the same analyte solution composition as for the cyclic voltammograms above. Bottom right: Plot of $|I|t^{1/2}$ vs $t^{1/2}$ of the data from the chronoamperometry of **1** fitted with a trend line (red).

and, thus, many more ^{1}H NMR signals than four for the *ate*-complex, it appears that the cyanide can readily move in between the two samarium atoms so that the phenylene bridges can easily move "over" the small coordinated anion at ambient temperature. The effective magnetic moment of complex **3** was calculated to be μ_{eff} = 2.00 μ_B. This value is lower than that calculated for **1** and might indicate antiferromagnetic coupling resulting from cyanide-mediated superexchange between the two samarium(III) ions. This difference may also be reflected in the diminished paramagnetic shifting of the ^{1}H NMR resonances in comparison with compound **1**. The crystalline material used for the NMR analysis was prepared by layering solutions of **3** in THF with diethyl ether, which is presumably the reason why the ^{1}H and ^{13}C NMR data shows 2 equiv of coordinated THF. Since the THF does not exhibit any paramagnetic shifting, it is most likely bound to the crown ether-embedded potassium ion forming the often observed $[K(18\text{-crown-}6)(THF)_2]^+$ moiety in which the coordinated potassium ion saturates the two apical positions with THF molecules.[31,32]

The UV−vis spectra (see Figures S11−S14) of the complexes are dominated by the absorptions of the bridging phenylenes in the range of ca. 245−280 nm. Here, **1** and **2** exhibit a very similar absorption behavior with three prominent maxima at 255, 261, and 273 nm for **1** and 257, 260, and 273 nm for **2**, whereas **3** shows narrower absorption bands with maxima at 247, 254, 261, 268, and 273 nm. This indicates that a broader distribution of different conformations with similar energies is present in solution at ambient temperature for complexes **1** and **2**, broadening the absorption bands. However, in the case of **3**, the distribution of different conformations is narrower by comparison, which suggests slightly higher energy differences for the accessible conformations of the complex. This appears feasible considering the effect of cyanide coordination to the arrangement of the ligand framework in the solid state. At higher wavelengths, **3** also exhibits weak peaks at 363 and 392 nm, which are not observed in the spectra for **1** and **2**.

Electrochemical Analyses. Cyclic voltammetry experiments for the three samarium complexes did not exhibit any redox process related to the Sm^{III}/Sm^{II} redox couple within the range of 0.8 to −3.5 V vs Fc^+/Fc. The measurements were performed using $^{n}Bu_4NBPh_4$ or $^{n}Bu_4NPF_6$ (100 mM) as the supporting electrolyte in THF at ambient temperature with ferrocene in the same concentration as the analyte (2 mM) (Figures 4 and S20−S24). To exclude the possibility of a broadened redox band, a chronoamperometric measurement of a quiescent solution of **1** was performed over the period of 60 s at a potential of −3.3 V vs Fc^+/Fc (Figure 4). This potential was chosen to avoid any reduction of the solvent or supporting electrolyte, so as to not confuse any such processes with the reduction of **1**. According to a published method,[33] the data was plotted in the form of $|I|t^{1/2}$ vs $t^{1/2}$ from which the number of transferred electrons per analyte molecule (n) was estimated to 1.1 × 10^{-2} (Figure 4, see p15 in the ESI for the calculation details). The calculated value is significantly lower than that expected for the reduction of one samarium(III) atom (n = 1) or both (n = 2). Therefore, we conclude that no analyte reduction occurs at a potential of −3.3 V. This further supports the observations from the cyclic voltammetry that the Sm^{III}/Sm^{II} redox couple is below the available measurement window in complex **1** and extends this conclusion to compounds **2** and **3**. For comparison, the Sm^{III}/Sm^{II} redox couple for $Sm[N(SiMe_3)_2]_3$ was reported for $E_{1/2}$ = −2.1 V.[34] However, in the case of the previously reported TREN-based europium complex $N[(CH_2)_2NCH(C_6H_2\text{-}4,6\text{-}^{t}Bu_2\text{-}2\text{-}O)]_3Eu$, the Eu^{III}/Eu^{II} redox couple, which is typically ca. 1 V higher than that of samarium, was observed only as a shoulder on the lower limit of the measurement window using similar conditions.[35]

CONCLUSIONS

In summary, we presented the synthesis of a dinuclear azacryptand samarium complex **1** by the aminolysis reaction

https://doi.org/10.1021/acs.inorgchem.1c03989
Inorg. Chem. 2022, 61, 5539−5546

from $Sm[N(SiMe_3)_2]_3$ and azacryptand H_6L in a 2:1 molar ratio. Changing the ratio to 1:1 yielded the monometallic samarium complex **2**. The solid-state structure of disamarium complex **1** exhibits a vacant space in between the two metal centers along with the available coordination sites, despite the presence of otherwise strongly binding THF. With this ideal situation for cooperative small molecule activation, we investigated the incorporation of cyanide, which is isoelectronic to dinitrogen and carbon monoxide, forming metal-bridging adducts. We characterized the complexes by NMR, UV−vis, and IR spectroscopy as well as electrochemical analysis and single-crystal X-ray diffraction and determined the effective magnetic moments using the Evans method. These are the first examples of azacryptand-based f-metal complexes and we demonstrate their ability to bind cyanide in the presence of strongly coordinating solvents like THF. Moreover, the selective monometallation opens a pathway to mixed metal complexes combining different properties and reactivities. Consequently, these complexes represent a novel platform for the investigation of cooperative small molecule activation using f-elements and other early metals.

EXPERIMENTAL SECTION

General Details. All manipulations were carried out under an atmosphere of dry, oxygen-free nitrogen using standard Schlenk and glovebox techniques. Benzene-d_6 was distilled from potassium, THF-d_8 was dried with potassium, and pyridine-d_5 degassed and dried over 4 Å molecular sieves. Dichloromethane and THF were purified by distillation from calcium hydride under nitrogen. All other solvents were purified by passing through columns of activated alumina.[36] Other chemicals were obtained from different suppliers and used without further purification. $N[(CH_2)_2NHCH_2(p\text{-}C_6H_4)CH_2NH(CH_2)_2]_3N$ (H_6L)[15] and $Sm[N(SiMe_3)_2]_3$[37] were prepared according to published procedures. The NMR spectra were recorded on a Varian INOVA 500 or a Bruker AVANCE III 300 and were referenced to Me_4Si (^1H, ^{13}C). The ^1H NMR data required for the Evans method calculations of the magnetic moments, μ_{eff}, were recorded using solutions of the analytes in pyridine-d_5 with and without a sealed capillary containing pyridine-d_5 to determine the shift differences between the solvent residue peaks.[29] The average values of the shift differences of all three pyridine-*d* resonances were used for the calculations.[38,39] For X-ray structure analyses, the crystals were mounted onto the tips of glass fibers. Data collection was performed with a Bruker-AXS SMART APEX CCD diffractometer using graphite-monochromated Mo Kα radiation (0.71073 Å). The data were reduced to F_o^2 and corrected for absorption effects with SAINT[40] and SADABS,[41,42] respectively. The structures were solved by direct methods and refined by the full-matrix least-squares method (SHELXL97 or SHELXL19).[43] If not noted otherwise, all non-hydrogen atoms were refined with anisotropic displacement parameters. All hydrogen atoms were located in calculated positions to correspond to standard bond lengths and angles. Crystallographic data for the structures reported in this paper have been deposited with the Cambridge Crystallographic Data Center as supplementary publication no. CCDC 2109128 (**1**), 2109129 (**2**), and 2109130 (**3**). UV−vis spectra were recorded on an Agilent Cary 60 UV−vis spectrophotometer using THF to prepare analyte solutions for the measurements. Elementary analysis was carried out using a Heraeus VARIO ELEMENTAR. IR data was recorded on a Bruker Alpha-T FTIR spectrometer. The electrochemical analyses were performed using a BioLogic SP-150 potentiostat. The measurements were made on 2 mM solutions of the analyte in 10 mL of THF using $^nBu_4NBPh_4$ or $^nBu_4NPF_6$ (100 mM) as the supporting electrolyte in a glovebox. Here, a glassy carbon working electrode (d = 3 mm), a Pt-wire counter electrode, and a Ag-wire quasi-reference electrode were used and the data referenced against ferrocenium/ferrocene (Fc^+/Fc = 0 V, 2 mM).

Syntheses. *Disamarium(III) Azacryptand Complex LSm_2 **1**.* A vial equipped with a stirrer bar was charged with **H_6L** (1.78 g, 2.97 mmol) and THF (5 mL) and a solution of $Sm[N(SiMe_3)_2]_3$ (4.12 g, 6.53 mmol) in THF (5 mL) was added dropwise to the ligand solution. The yellow reaction mixture was filtered and heated to 70 °C for 5 h under vigorous stirring during which a bright yellow precipitate formed. After cooling to ambient temperature, the supernatant dark brown solution was decanted and the precipitate was washed four times with THF (5 mL) and one more time with Et_2O (4 mL). The bright yellow solid was then dried under reduced pressure yielding 1.02 g (38%) of **1**. mp. 248 °C (dec.). ^1H NMR (δ in ppm, benzene-d_6, 298 K): −10.23 (br s, 12H, CH_2), −3.06 (br s, 12H, CH_2), 6.53 (br s, 12H, CH_2). μ_{eff} = 2.35 μ_B. UV−vis: $\lambda_{max,1}$ = 249 nm ($\varepsilon_1 = 1.4 \times 10^4$ L mol^{-1} cm^{-1}, shoulder), $\lambda_{max,2}$ = 255 nm ($\varepsilon_2 = 1.2 \times 10^4$ L mol^{-1} cm^{-1}), $\lambda_{max,3}$ = 261 nm ($\varepsilon_3 = 1.1 \times 10^4$ L mol^{-1} cm^{-1}), $\lambda_{max,4}$ = 264 nm ($\varepsilon_4 = 1.0 \times 10^3$ L mol^{-1} cm^{-1}, shoulder), $\lambda_{max,5}$ = 273 nm ($\varepsilon_5 = 7.3 \times 10^3$ L mol^{-1} cm^{-1}, shoulder), $\lambda_{max,6}$ = 306 nm ($\varepsilon_6 = 2.2 \times 10^3$ L mol^{-1} cm^{-1}, shoulder), $\lambda_{max,7}$ = 338 nm ($\varepsilon_7 = 1.3 \times 10^3$ L mol^{-1} cm^{-1}, shoulder). IR (ATR, cm^{-1}): 402, 422, 454, 503, 558, 625, 714, 742, 812, 842, 864, 904, 923, 964, 1017, 1044, 1047, 1098, 1127, 1146, 1184, 1224, 1254, 1289, 1317, 1341, 1436, 1454, 1501, 2119, 2340, 2687, 2742, 2789, 2808, 2876, 2939, 3013, 3275. Analysis calcd for $C_{36}H_{48}N_8Sm_2$ [893.56]: C 48.39, H 5.41, N 12.54. Found: C 48.73, H 5.25, N 12.53.

*Samarium(III) Azacryptand Complex H_3LSm **2**.* A vial equipped with a stirrer bar was charged with **H_6L** (598 mg, 1.00 mmol), $Sm[N(SiMe_3)_2]_3$ (632 mg, 1.00 mmol), and THF (3 mL). The vial was sealed and then heated to 70 °C for 18 h. Then the dark brown mixture was allowed to cool to ambient temperature and orange crystals of **2** formed. The solution was then decanted and the orange crystals washed with diethyl ether yielding 500 mg (76%) of **2**. mp 232 °C (dec.). ^1H NMR (δ in ppm, benzene-d_6, 298 K): −8.00 (br, 6H, CH_2), −1.89 (s, 3H, NH), −1.29 (br, 6H, CH_2), 1.25 (s, 12H, CH_2), 1.65 (br, 6H, CH_2), 4.24 (d, J = 7 Hz, 6H, CH), 7.80 (s, 6H, CH_2), 11.37 (d, J = 5 Hz, 6H, CH). $^{13}C\{^1H\}$ NMR (δ in ppm, benzene-d_6, 298 K): 45.9, 50.5, 51.5, 66.1, 81.0, 124.4, 135.9, 145.3. μ_{eff} = 1.80 μ_B. UV−vis: $\lambda_{max,1}$ = 247 nm ($\varepsilon_1 = 1.4 \times 10^4$ L mol^{-1} cm^{-1}, shoulder), $\lambda_{max,2}$ = 254 nm ($\varepsilon_2 = 1.2 \times 10^4$ L mol^{-1} cm^{-1}), $\lambda_{max,3}$ = 260 nm ($\varepsilon_3 = 1.0 \times 10^4$ L mol^{-1} cm^{-1}), $\lambda_{max,4}$ = 264 nm ($\varepsilon_4 = 9.8 \times 10^3$ L mol^{-1} cm^{-1}, shoulder), $\lambda_{max,5}$ = 273 nm ($\varepsilon_5 = 7.0 \times 10^3$ L mol^{-1} cm^{-1}), $\lambda_{max,6}$ = 298 nm ($\varepsilon_6 = 2.3 \times 10^3$ L mol^{-1} cm^{-1}). IR (ATR, cm^{-1}): 390, 415, 489, 546, 570, 602, 619, 677, 721, 748, 784, 804, 845, 863, 911, 935, 973, 1019, 1054, 1069, 1098, 1125, 1138, 1197, 1211, 1223, 1258, 1281, 1292, 1325, 1363, 1384, 1418, 1439, 1452, 1509, 1611, 1648, 1802, 1902, 2080, 2695, 2731, 2799, 2875, 2946, 3015, 3093, 3281, 3610. Analysis calcd for $C_{36}H_{51}N_8Sm$ [746.22]: C 57.93, H 6.89, N 15.02. Found: C 58.88, H 6.71, N 14.63.

*Disamarium(III) Azacryptand Complex Cyanide Adduct $[LSm_2CN][K(18\text{-Crown-}6)(THF)_2]$ **3**.* A vial equipped with a stirrer bar was charged with **1** (180 mg, 0.20 mmol), 18-crown-6 (53 mg, 0.20 mmol), potassium cyanide (13 mg, 0.20 mmol), and THF (4 mL). The reaction mixture was heated to 70 °C for 2 h during which the initial yellow suspension turned into a clear orange-brown solution. Then the solvent was evaporated under reduced pressure and the brown residue crystallized from THF and Et_2O at −50 °C yielding yellow crystals of **3** (0.21 g, 86%). mp 102 °C (dec.). ^1H NMR (δ in ppm, THF-d_8, 298 K): −4.91 (br, 12H, CH_2), −0.14 (br, 12H, CH_2), 1.78 (m, 8H, THF), 3.61 (m, 8H, THF), 3.92 (s, 24H, 18-crown-6), 5.13 (br, 12H, CH), 5.97 (s, 12H, CH_2). $^{13}C\{^1H\}$ NMR (δ in ppm, THF-d_8, 298 K): 26.4, 46.0, 65.4, 68.3, 71.6, 73.9, 127.7, 144.1. μ_{eff} = 2.00 μ_B. UV−vis: $\lambda_{max,1}$ = 247 nm ($\varepsilon_1 = 1.4 \times 10^4$ L mol^{-1} cm^{-1}), $\lambda_{max,2}$ = 254 nm ($\varepsilon_2 = 1.2 \times 10^4$ L mol^{-1} cm^{-1}), $\lambda_{max,3}$ = 261 nm ($\varepsilon_3 = 1.1 \times 10^4$ L mol^{-1} cm^{-1}), $\lambda_{max,4}$ = 268 nm ($\varepsilon_4 = 8.9 \times 10^3$ L mol^{-1} cm^{-1}), $\lambda_{max,5}$ = 272 nm ($\varepsilon_5 = 7.1 \times 10^3$ L mol^{-1} cm^{-1}, shoulder), $\lambda_{max,6}$ = 291 nm ($\varepsilon_6 = 2.8 \times 10^3$ L mol^{-1} cm^{-1}, shoulder), $\lambda_{max,7}$ = 305 nm ($\varepsilon_7 = 2.0 \times 10^3$ L mol^{-1} cm^{-1}, shoulder), $\lambda_{max,8}$ = 363 nm ($\varepsilon_8 = 9.1 \times 10^2$ L mol^{-1} cm^{-1}), $\lambda_{max,9}$ = 392 nm ($\varepsilon_9 = 6.6 \times 10^2$ L mol^{-1} cm^{-1}). IR (ATR, cm^{-1}): 377, 400, 496, 529, 560, 621, 750, 806, 843, 867, 907, 958, 1056, 1101, 1203, 1246, 1281, 1326, 1349, 1376, 1408, 1437, 1451, 1470, 1506, 2058, 2115, 2630, 2694, 2739,

https://doi.org/10.1021/acs.inorgchem.1c03989
Inorg. Chem. 2022, 61, 5539−5546

2769, 2814, 2864, 2885, 2942, 3048. Analysis calcd for $C_{49}H_{72}KN_9O_6Sm_2$ [1222.99]: C 48.12, H 5.93, N 10.31. Found: C 48.35, H 5.20, N 10.42.

N[(CH$_2$)$_2$NHCH$_2$-p-C$_6$H$_4$CH$_2$NH(CH$_2$)$_2$]$_3$N H$_6$L.[15] Additional analytical data: ^{1}H NMR (δ in ppm, benzene-d_6, 298 K): 1.71 (quint, 6H, $^3J_{HH}$ = 8 Hz, NH), 2.43 (m, 12H, CH$_2$), 2.65 (m, 12H, CH$_2$), 3.67 (d, 12H, $^3J_{HH}$ = 8 Hz, ArCH$_2$) 7.07 (s, 12H, CH). ^{1}H NMR (δ in ppm, chloroform-d, 298 K): 1.72 (br s, 6H, NH), 2.65 (m, 12H, CH$_2$), 2.81 (m, 12H, CH$_2$), 3.67 (s, 12H, ArCH$_2$) 6.87 (s, 12H, CH). Couplings to amine protons were only observed for data recorded of solutions in benzene-d_6. ^{13}C{^{1}H} NMR (δ in ppm, benzene-d_6, 298 K): 48.2, 53.5, 54.7, 127.8, 139.4. ^{13}C{^{1}H} NMR (δ in ppm, chloroform-d, 298 K, APT): 48.0, 53.6, 54.3, 127.5, 139.6. UV−vis: $\lambda_{max,1}$ = 257 nm (ε_1 = 1.1 × 10^4 L mol^{-1} cm^{-1}), $\lambda_{max,2}$ = 264 nm (ε_2 = 1.1 × 10^4 L mol^{-1} cm^{-1}), $\lambda_{max,3}$ = 267 nm (ε_3 = 1.0 × 10^4 L mol^{-1} cm^{-1}, shoulder), $\lambda_{max,4}$ = 273 nm (ε_4 = 7.3 × 10^3 L mol^{-1} cm^{-1}), $\lambda_{max,5}$ = 331 nm (ε_5 = 6.0 × 10^2 L mol^{-1}cm^{-1}). IR (ATR, cm^{-1}): 393, 491, 592, 738, 7725, 799, 864, 884, 920, 974, 1019, 1054, 1098, 1127, 1160, 1224, 1291, 1328, 1359, 1387, 1431, 1450, 1515, 1671, 1910, 2084, 2654, 2734, 2798, 2880, 2943, 3010, 3228, 3271, 3283, 3306.

■ ASSOCIATED CONTENT

Supporting Information

The Supporting Information is available free of charge at https://pubs.acs.org/doi/10.1021/acs.inorgchem.1c03989.

Additional electronic supporting information includes crystallographic data, NMR, UV−vis, and IR spectroscopic data as well as electrochemical analyses of the presented compounds (PDF)

Accession Codes

CCDC 2109128−2109130 contain the supplementary crystallographic data for this paper. These data can be obtained free of charge via www.ccdc.cam.ac.uk/data_request/cif, or by emailing data_request@ccdc.cam.ac.uk, or by contacting The Cambridge Crystallographic Data Centre, 12 Union Road, Cambridge CB2 1EZ, UK; fax: +44 1223 336033.

■ AUTHOR INFORMATION

Corresponding Author

Johann A. Hlina − *Institute of Inorganic Chemistry, Graz University of Technology, 8010 Graz, Austria;* orcid.org/0000-0001-9329-4180; Email: johann.hlina@tugraz.at.

Authors

Johanna M. Uher − *Institute of Inorganic Chemistry, Graz University of Technology, 8010 Graz, Austria*

Matthias R. Steiner − *Institute of Inorganic Chemistry, Graz University of Technology, 8010 Graz, Austria*

Complete contact information is available at: https://pubs.acs.org/10.1021/acs.inorgchem.1c03989

Funding

Open Access is funded by the Austrian Science Fund (FWF).

Notes

The authors declare no competing financial interest.

■ ACKNOWLEDGMENTS

The authors thank Christoph Marschner and Judith Baumgartner for support and helpful discussions, Hansjörg Weber for help with NMR specroscopy, and the Fonds zur Förderung der wissenschaftlichen Forschung (FWF) for financial support via project P 32005 and Graz University of Technology for funding via the Initial Funding Program (10th call).

■ REFERENCES

(1) Werkema, E. L.; Maron, L.; Eisenstein, O.; Andersen, R. A. Reactions of Monomeric [1,2,4-(Me$_3$C)$_3$C$_5$H$_2$]$_2$CeH and CO with or without H$_2$: An Experimental and Computational Study. *J. Am. Chem. Soc.* **2007**, *129*, 2529−2541.

(2) Arnold, P. L.; Turner, Z. R.; Bellabarba, R. M.; Tooze, R. P. Carbon Monoxide Coupling and Functionalisation at a Simple Uranium Coordination Complex. *Chem. Sci.* **2011**, *2*, 77−79.

(3) Fang, M.; Farnaby, J. H.; Ziller, J. W.; Bates, J. E.; Furche, F.; Evans, W. J. Isolation of $(CO)^{1-}$ and $(CO_2)^{1-}$ Radical Complexes of Rare Earths via Ln(NR$_2$)$_3$/K Reduction and [K$_2$(18-Crown-6)$_2$]$^{2+}$ Oligomerization. *J. Am. Chem. Soc.* **2012**, *134*, 6064−6067.

(4) Tsoureas, N.; Summerscales, O. T.; Cloke, F. G. N.; Roe, S. M. Steric Effects in the Reductive Coupling of CO by Mixed-Sandwich Uranium(III) Complexes. *Organometallics* **2013**, *32*, 1353−1362.

(5) Summerscales, O. T.; Cloke, F. G. N.; Hitchcock, P. B.; Green, J. C.; Hazari, N. Reductive Cyclotrimerization of Carbon Monoxide to the Deltate Dianion by an Organometallic Uranium Complex. *Science* **2006**, *311*, 829−831.

(6) Summerscales, O. T.; Cloke, F. G. N.; Hitchcock, P. B.; Green, J. C.; Hazari, N. Reductive Cyclotetramerization of CO to Squarate by a U(III) Complex: The X-Ray Crystal Structure of [(U(η-C$_8$H$_6${Si^{i}Pr$_3$-1,4}$_2$)(η-C$_5$Me$_4$H)]$_2$(μ-η^2:η^2-C$_4$O$_4$). *J. Am. Chem. Soc.* **2006**, *128*, 9602−9603.

(7) Evans, W. J.; Ulibarri, T. A.; Ziller, J. W. Isolation and X-Ray Crystal Structure of the First Dinitrogen Complex of an f-Element Metal, [(C$_5$Me$_5$)$_2$Sm]$_2$N$_2$. *J. Am. Chem. Soc.* **1988**, *110*, 6877−6879.

(8) Cloke, F. G. N.; Hitchcock, P. B. Reversible Binding and Reduction of Dinitrogen by a Uranium(III) Pentalene Complex. *J. Am. Chem. Soc.* **2002**, *124*, 9352−9353.

(9) Woen, D. H.; Chen, G. P.; Ziller, J. W.; Boyle, T. J.; Furche, F.; Evans, W. J. End-On Bridging Dinitrogen Complex of Scandium. *J. Am. Chem. Soc.* **2017**, *139*, 14861−14864.

(10) Benndorf, P.; Schmitt, S.; Köppe, R.; Oña-Burgos, P.; Scheurer, A.; Meyer, K.; Roesky, P. W. Catching Gaseous SO2 in Cone-Type Lanthanide Complexes: An Unexpected Coordination Mode for SO2 in f-Element Chemistry. *Angew. Chem., Int. Ed.* **2012**, *51*, 5006−5010.

(11) Arnold, P. L.; Hollis, E.; White, F. J.; Magnani, N.; Caciuffo, R.; Love, J. B. Single-Electron Uranyl Reduction by a Rare-Earth Cation. *Angew. Chem., Int. Ed.* **2011**, *50*, 887−890.

(12) Arnold, P. L.; Hollis, E.; Nichol, G. S.; Love, J. B.; Griveau, J.-C.; Caciuffo, R.; Magnani, N.; Maron, L.; Castro, L.; Yahia, A.; Odoh, S. O.; Schreckenbach, G. Oxo-Functionalization and Reduction of the Uranyl Ion through Lanthanide-Element Bond Homolysis: Synthetic, Structural, and Bonding Analysis of a Series of Singly Reduced Uranyl−Rare Earth 5f^1-4f^n Complexes. *J. Am. Chem. Soc.* **2013**, *135*, 3841−3854.

(13) Arnold, P. L.; Stevens, C. J.; Bell, N. L.; Lord, R. M.; Goldberg, J. M.; Nichol, G. S.; Love, J. B. Multi-Electron Reduction of Sulfur and Carbon Disulfide Using Binuclear Uranium(III) Borohydride Complexes. *Chem. Sci.* **2017**, *8*, 3609−3617.

(14) Cowie, B. E.; Douair, I.; Maron, L.; Love, J. B.; Arnold, P. L. Selective Oxo Ligand Functionalisation and Substitution Reactivity in an Oxo/Catecholate-Bridged U^{IV}/U^{IV} Pacman Complex. *Chem. Sci.* **2020**, *11*, 7144−7157.

(15) Jazwinski, J.; Lehn, J.-M.; Lilienbaum, D.; Ziessel, R.; Guilhem, J.; Pascard, C. Polyaza Macrobicyclic Cryptands: Synthesis, Crystal Structures of a Cyclophane Type Macrobicyclic Cryptand and of Its Dinuclear Copper(I) Cryptate, and Anion Binding Features. *J. Chem. Soc., Chem. Commun.* **1987**, *22*, 1691−1694.

(16) Möller, F.; Castañeda-Losada, L.; Junqueira, J. R. C.; Miller, R. G.; Reback, M. L.; Mallick, B.; van Gastel, M.; Apfel, U.-P. Modulation of the CO_2 Fixation in Dinickel Azacryptands. *Dalton Trans.* **2017**, *46*, 5680−5688.

(17) King, D. M.; Tuna, F.; McInnes, E. J. L.; McMaster, J.; Lewis, W.; Blake, A. J.; Liddle, S. T. Synthesis and Structure of a Terminal Uranium Nitride Complex. *Science* **2012**, *337*, 717−720.

(18) Damon, P. L.; Wu, G.; Kaltsoyannis, N.; Hayton, T. W. Formation of a Ce(IV) Oxo Complex via Inner Sphere Nitrate Reduction. *J. Am. Chem. Soc.* **2016**, *138*, 12743−12746.
(19) Gardner, B. M.; Stewart, J. C.; Davis, A. L.; McMaster, J.; Lewis, W.; Blake, A. J.; Liddle, S. T. Homologation and Functionalization of Carbon Monoxide by a Recyclable Uranium Complex. *Proc. Natl. Acad. Sci. U.S.A.* **2012**, *109*, 9265−9270.
(20) Feng, G.; Zhang, M.; Shao, D.; Wang, X.; Wang, S.; Maron, L.; Zhu, C. Transition-Metal-Bridged Bimetallic Clusters with Multiple Uranium−Metal Bonds. *Nat. Chem.* **2019**, *11*, 248−253.
(21) Alvarez, S. A Cartography of the van Der Waals Territories. *Dalton Trans.* **2013**, *42*, 8617−8636.
(22) El-Khatib, F.; Cahier, B.; Shao, F.; López-Jordà, M.; Guillot, R.; Rivière, E.; Hafez, H.; Saad, Z.; Girerd, J.-J.; Guihéry, N.; Mallah, T. Design and Magnetic Properties of a Mononuclear Co(II) Single Molecule Magnet and Its Antiferromagnetically Coupled Binuclear Derivative. *Inorg. Chem.* **2017**, *56*, 4601−4608.
(23) Evans, W. J.; Drummond, D. K. Reactivity of Isocyanides with $(C_5Me_5)_2Sm(THF)_2$: Synthesis and Structure of Trimeric $[(C_5Me_5)_2Sm(CNC_6H_{11})(\mu\text{-}CN)]_3$. *Organometallics* **1988**, *7*, 797−802.
(24) Obora, Y.; Ohta, T.; Stern, C. L.; Marks, T. J. Organolanthanide-Catalyzed Imine Hydrogenation. Scope, Selectivity, Mechanistic Observations, and Unusual Byproducts. *J. Am. Chem. Soc.* **1997**, *119*, 3745−3755.
(25) Evans, W. J.; Forrestal, K. J.; Ziller, J. W. Reaction Chemistry of Sterically Crowded Tris(Pentamethylcyclopentadienyl)Samarium [1]. *J. Am. Chem. Soc.* **1998**, *120*, 9273−9282.
(26) Evans, W. J.; Montalvo, E.; Foster, S. E.; Harada, K. A.; Ziller, J. W. Reactivity of $(C_5Me_5)_2Sm(THF)_2$ with Nitriles: C−C Bond Cleavage To Form Cyanide Complexes. *Organometallics* **2007**, *26*, 2904−2910.
(27) Gardiner, M. G.; James, A. N.; Jones, C.; Schulten, C. Sm(II) Reduction Chemistry of Heteroalkynes: Stable Adducts, Reductive Coupling, Reductive C−C/C−N Bond Cleavage and Trapping of the Tert-Butyl Fragment with Bulky Nitriles, Phosphaalkynes and Isonitriles. *Dalton Trans.* **2010**, *39*, 6864−6870.
(28) Liu, F.; Wang, S.; Gao, C.-L.; Deng, Q.; Zhu, X.; Kostanyan, A.; Westerström, R.; Jin, F.; Xie, S.-Y.; Popov, A. A.; Greber, T.; Yang, S. Mononuclear Clusterfullerene Single-Molecule Magnet Containing Strained Fused-Pentagons Stabilized by a Nearly Linear Metal Cyanide Cluster. *Angew. Chem., Int. Ed.* **2017**, *56*, 1830−1834.
(29) Schubert, E. M. Utilizing the Evans Method with a Superconducting NMR Spectrometer in the Undergraduate Laboratory. *J. Chem. Educ.* **1992**, *69*, 62.
(30) Greenwood, N. N.; Earnshaw, A. *Chemistry of the Elements*, 2nd ed.; Butterworth-Heinemann: Oxford; Boston, 1997.
(31) Duhme, A.-K.; Strasdeit, H. Controlled Degradation of a Ligand-Deficient Complex: From $[Cd(C_6F_5)(STrt)_4]$ to $[Cd(C_6F_5)(STrt)_3(OH)]^-$ and $[Cd(C_6F_5)(STrt)_2]^-$ (Trt = Triphenylmethyl). *Eur. J. Inorg. Chem.* **1998**, *1998*, 657−662.
(32) Balatoni, I.; Hlina, J.; Zitz, R.; Pöcheim, A.; Baumgartner, J.; Marschner, C. Disilene Fluoride Adducts versus β-Halooligosilanides. *Inorg. Chem.* **2019**, *58*, 14185−14192.
(33) Yap, W. T.; Doane, L. M. Determination of Diffusion Coefficients by Chronoamperometry with Unshielded Planar Stationary Electrodes. *Anal. Chem.* **1982**, *54*, 1437−1439.
(34) Prasad, E.; Knettle, B. W.; Flowers, R. A. Investigation of the $[Sm\{N(SiMe_3)_2\}_2]$ Reducing System in THF. Rate and Mechanistic Studies. *J. Am. Chem. Soc.* **2002**, *124*, 14663−14667.
(35) Lionetti, D.; Day, V. W.; Blakemore, J. D. Noncovalent Immobilization and Surface Characterization of Lanthanide Complexes on Carbon Electrodes. *Dalton Trans.* **2017**, *46*, 11779−11789.
(36) Pangborn, A. B.; Giardello, M. A.; Grubbs, R. H.; Rosen, R. K.; Timmers, F. J. Safe and Convenient Procedure for Solvent Purification. *Organometallics* **1996**, *15*, 1518−1520.
(37) Schuetz, S. A.; Day, V. W.; Sommer, R. D.; Rheingold, A. L.; Belot, J. A. Anhydrous Lanthanide Schiff Base Complexes and Their Preparation Using Lanthanide Triflate Derived Amides. *Inorg. Chem.* **2001**, *40*, 5292−5295.
(38) Piguet, C. Paramagnetic Susceptibility by NMR: The "Solvent Correction" Removed for Large Paramagnetic Molecules. *J. Chem. Educ.* **1997**, *74*, 815−816.
(39) Bain, G. A.; Berry, J. F. Diamagnetic Corrections and Pascal's Constants. *J. Chem. Educ.* **2008**, *85*, 532.
(40) *SAINTPLUS: Software Reference Manual*, version 6.45, Bruker-AXS: Madison,WI, 1997-2003.
(41) Blessing, R. H. An Empirical Correction for Absorption Anisotropy. *Acta Crystallogr., Sect. A: Found. Crystallogr.* **1995**, *51*, 33−38.
(42) Sheldrick, G. M. *SADABS*, Bruker AXS Inc.: Madison, WI, 2003.
(43) Sheldrick, G. M. A Short History of *SHELX*. *Acta Crystallogr., Sect. A: Found. Crystallogr.* **2008**, *64*, 112−122.

https://doi.org/10.1021/acs.inorgchem.1c03989
Inorg. Chem. 2022, 61, 5539−5546